JOINT INSTITUTE FOR NUCLEAR RESEARCH
Frank Laboratory of Neutron Physics
Sector of Research of Neutron-Nuclear Interactions

FINAL REPORT ON THE START PROGRAMME

Study of the characteristics of BGO γ-detectors at the «Gamma-7» facility

Supervisor:
Dr. Natalia Viktorovna Rebrova
Dr. Valery Leonidovich Kuznetsov

Student:
Rustam Akmaletdinov, Russian Federation
Ural Federal University named after the first President of Russia B. N. Yeltsin (UrFU)

Participation period:
July 27 – September 6,
Summer Session 2025

Dubna, 2025

Contents

Introduction

This work addresses the experimental investigation of the characteristics of the Gamma-7 prototype, which consists of scintillation γ-detectors based on bismuth germanate (BGO) crystals, with the aim of accounting for operational features and guiding the staged development of the setup.

The report presents results in the following areas carried out on Gamma-7: time-of-flight spectra and calibration; identification of lines in spectra from a neutron source; and the influence of count rate (load) on the characteristics of Gamma-7. We also report studies of the temperature dependence of efficiency and the determination of the detection efficiency and energy resolution of the BGO scintillation detector.

The experimental part of the studies was performed at IREN (the Intense Resonance Neutron Source) of the I. M. Frank Laboratory of Neutron Physics, JINR. IREN is a pulsed neutron source based on the LUE-200 electron linear accelerator and currently operates in test mode [1].

The Gamma-7 setup is located on the 10 m flight path of IREN's channel 4. On this detector system, studies are conducted of the elemental composition of samples by the method of neutron resonance analysis, as well as of the angular distributions of γ rays emitted in radiative neutron capture. Analysis of experimental data, assessment of feasibility, and planning of experiments on Gamma-7 require knowledge of the setup's characteristics: energy resolution, detection efficiency, and the dependence of detector parameters on temperature and count rate.

In the course of this work, practical experience was also gained with application software in the Linux Mint environment. In particular, the Romana program [2], developed at the Joint Institute for Nuclear Research for the accumulation, analysis, and visualization of experimental data, was used. Origin [3] was employed for the processing and visualization of experimental spectra.

1 Theoretical Overview

1.1 Neutron Sources

Neutron sources are widely used in fundamental and applied research. For practical applications, neutron sources are required that have small dimensions, stable radiation output, relatively low cost, isotropic emission, and relative ease of use.

In such portable neutron sources, the $^{9}\mathrm{Be}(\alpha, \mathrm{n})^{12}\mathrm{C}$ reaction is widely employed.

Certified Am-241/Be neutron sources are a compacted mixture of americium oxide $^{241}\mathrm{AmO}_2$ and metallic beryllium powders BeO pressed into a cylindrical form to increase the probability of α-particle interactions with beryllium and sealed in a single- or double-walled stainless-steel capsule.

The radioactive isotope Am-241 is unstable and has a half-life of 432.6 years. In its decay, americium-241 emits α particles, while the daughter nuclide neptunium-237 emits a cascade of γ rays and/or conversion electrons:

$$^{241}_{95}\mathrm{Am} \rightarrow {}^{237}_{93}\mathrm{Np} + {}^{4}_{2}\alpha\,.$$

The α-activity of the sources is determined primarily by the decay of americium-241, since neptunium-237 is the longest-lived neptunium isotope, with a half-life of $2.144 \cdot 10^{6}$ years, decaying to protactinium-233. The active part of such a certified source produces an average neutron flux on the order of $5 \cdot 10^{4} \div 5 \cdot 10^{5}$ neutrons/s [4].

The α particles emitted by americium-241 interact with beryllium-9 to produce neutrons. In the spectra of these sources, lines appear at 2.223 MeV and 4.438 MeV, corresponding respectively to γ rays from neutron capture on protons and from excited states of carbon-12. Moderators are used to slow fast neutrons down into the thermal energy range.

Part of the experiments was carried out at the Intense Resonance Neutron Source (IREN) at the Laboratory of Neutron Physics. IREN is a photoneutron source in which neutrons are produced via the (γ, n) reaction. Bremsstrahlung is generated by the LUE-200 electron linear accelerator. A tungsten-based alloy, VNZh-90, is used as the non-multiplying neutron-production target material. The target dimensions are $\emptyset\ 40\text{мм} \times 100\text{мм}$ [1]. The accelerated electron beam strikes the tungsten target; in the strong Coulomb field of W nuclei the electrons lose energy, emitting bremsstrahlung γ rays. Neutrons are then produced through interactions of these γ rays with tungsten nucleus:

$$\gamma + {}^{A}\mathrm{W} \rightarrow {}^{A-1}\mathrm{W} + n\,.$$

To moderate fast neutrons to thermal energies, the production target is surrounded by 50 mm of distilled water. A collimator defines the neutron beam at a small solid angle and reduces background.

1.2 Gamma-Ray Interactions with Matter

1.2.1 Principal Processes of Gamma-Ray Interaction with Matter

The scintillation method of particle detection is based on converting the energy of γ rays into light flashes produced in certain materials called scintillators. As γ rays pass through a scintillator, a number of physical processes occur, leading to attenuation of the intensity of the primary γ-ray beam. The principal interaction mechanisms are:

1. The photoelectric effect;

2. Compton scattering;

3. Electron–positron pair production.

These processes are governed by electronic transitions in the crystal's luminescence (scintillation) centers.

Their corresponding cross sections σ_{ph}, σ_C, σ_{pair} dd to give the total interaction cross section:

$$\sigma = \sigma_{ph} + \sigma_C + \sigma_{pair},$$

where each term has a different dependence on the γ-ray energy E_γ and on Z.

At low photon energies (up to a few hundred keV), photoelectric absorption of the γ quantum (the photoelectric effect) dominates. In the photoelectric process within the scintillator crystal, the ejected electron acquires kinetic energy

$$E_e = E_\gamma - E_{\text{яд}} - I_i,$$

where E_γ is the γ-ray energy; I_i – is the ionization energy of the electron from the i-th shell ($i = K, L, M\ldots$); and E_{nuc} is the nuclear recoil energy. The vacancy created in an inner atomic shell is filled by an electron from a higher shell (L or M). The energy released is carried away either by characteristic X-rays or by Auger electrons. Both have relatively low energies and are mostly absorbed within the detector. As a result of full absorption of the γ-ray energy in the detector's sensitive volume, the deposited energy is converted into excitation of the scintillator atoms, producing a scintillation flash. In the amplitude spectrum this appears as a single peak—the photopeak (full-energy peak) [5].

The effective photoelectric cross section σ_{ph} depends on the γ-ray energy and on the absorber's atomic number Z:

$$\sigma_{\mathrm{ph}} \sim Z^5.$$

At higher photon energies E_γ the photoelectric-effect cross section σ_{ph} is small compared to other processes.

Compton scattering is the interaction of a γ quantum of energy $E_\gamma = h\nu$ with a stationary electron, as a result of which the electron acquires a recoil momentum and the corresponding kinetic energy:

$$E_e = E_\gamma - \mathrm{E}_{\gamma'},$$

$$\mathrm{E}_{\gamma'} = \frac{E_\gamma}{1 + \varepsilon(1 - \cos\theta)},$$

where E_γ, E'_γ are the γ-ray energies before and after scattering; θ is the γ-ray scattering angle; and E_e – is the electron kinetic energy.

The total Compton-scattering cross section σ_C is proportional to Z:

$$\sigma_{\mathrm{C}} \sim Z.$$

In the spectrum of γ radiation from the Cs-137 isotope, the full-energy peak appears at E_γ = 661.7 keV. To its right, a full-energy peak will be observed at $E_e = 478\ keV$. The pronounced peak at the very beginning of the spectrum is formed by the Cs-137 X-ray emission at 33 keV.

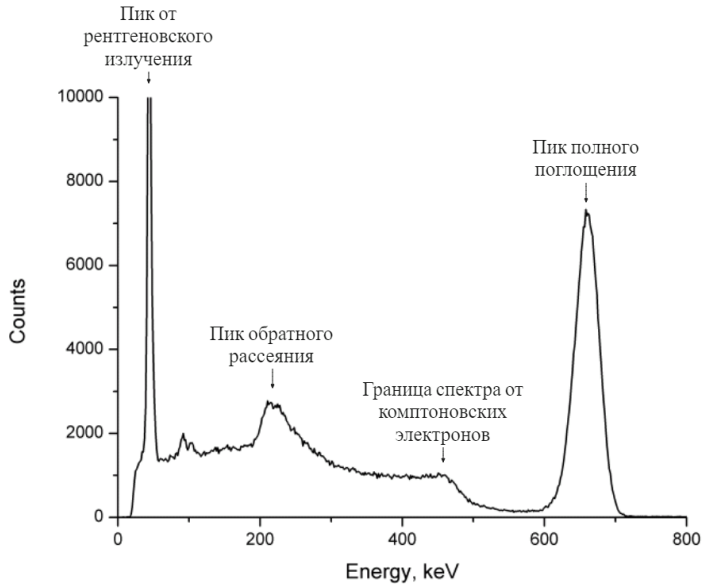

Figure 1 – Amplitude spectrum from pulses of γ quant ^{137}Cs .

At energies $E_\gamma > 2m_e c^2 = 1.02\,MeV$ the process of electron–positron pair production becomes possible. Once in matter, the positron almost completely loses its velocity due to ionization losses, so immediately before annihilation it can be regarded as being at rest. The fate of the overwhelming majority of pairs is annihilation, which proceeds with the emission of two γ quanta of energy $m_e c^2 = 0.511\ MeV$ emitted in opposite directions. If one of the γ quanta is fully absorbed in the crystal, a single-escape peak at $E_\gamma = 0.511$ МэВ formed. The escape of both γ quanta from the scintillator corresponds to a double-escape peak in the spectrum at $E_\gamma =$ 1.02 МэВ.

The total cross section for the pair-production effect σ_{pair} is proportional to the square of the nuclear charge Z:

$$\sigma_{pair} \sim Z^2.$$

Thus, the principal processes of γ-radiation interaction with matter listed above provide the theoretical basis for the subsequent analysis of the properties of the scintillation detectors used in this work.

1.2.2 The Role of Scintillation Detectors in Gamma-Ray Detection

One of the principal advantages of scintillation detectors over other types is their high efficiency for registering γ rays and neutrons. In our «Gamma-7» setup we use BDEG-1307-2 γ-radiation scintillation detection modules based on a bismuth germanate crystal $Bi_4Ge_3O_{12}$ (BGO) with a diameter and height of Ø 89мм × 265 mm. The properties of the detection system directly affect the results obtained. BGO detectors have a relatively low light yield and, consequently, poorer resolution than NaI(Tl) detectors. However, owing to their high density, they provide better detection efficiency for high-energy γ rays.

The Scintillator crystal	Z_{ef}	**Light output, photon/keV**	**Energy resolution**	**Thermal neutron activation**	**Density,** g/cm^3
NaI(Tl)	51	$4 \cdot 10^4$ photons per MeV	8.5 % at the Cs-137 line for a 50×150 mm detector	high	3.67
BGO	75	10 ÷ 12% of the NaI(Tl) yield	11 % at the Cs-137 line for a 56×130 mm detector	negligible	7.13

Table 1 – Basic physical characteristics of scintillation detectors..

The interaction of γ rays with matter is probabilistic and depends both on the properties of the γ radiation (its energy) and on the material in which the interaction occurs, including its density and elemental composition. Thus, for a single event it is impossible to predict what fraction of the γ-quantum's energy will be absorbed in the detector and what fraction will pass without any interaction. However, the statistical distribution of energies recorded by the detector can be determined by accumulating a large number of events—the distribution of the energies of the detected pulses from a monoenergetic source. This distribution is called the response function. The distribution of pulse amplitudes in the full-energy-peak region is described by a normal (Gaussian) distribution:

$$N(x) = P \cdot \frac{1}{\sqrt{2\pi\sigma^2}} \exp\left(-\frac{(x-M)^2}{2\sigma^2} \right),$$

where x is a random variable with mean M and variance σ^2; P – is the total number of registered pulses in the peak, i.e., the area under the peak; σ is the standard deviation of the normal distribution; M is the peak position on the argument scale xxx, which here is the channel number in the spectrum.

The peak width Δx at half maximum:

$$\Delta x = \sqrt{2\ln 2}\sigma \approx 2.354\sigma.$$

In practice, when analyzing amplitude distributions, one often uses the half-width at half maximum (HWHM):

$$\mathrm{HWHM} = \sqrt{2\ln 2}\sigma \approx 1.18\sigma.$$

In this work, reference spectrometric γ-ray sources (OSGI) were used: ^{137}Cs, ^{60}Co, ^{226}Th .

Cobalt-60:

$$^{60}_{27}\mathrm{Co} \xrightarrow[T_{1/2}=5.271\ \text{years}]{\beta^-} {}^{60}_{28}\mathrm{Ni}^* + e^- + \bar{\nu}_e,$$

$$^{60}_{28}\mathrm{Ni}^*(2505.7) \rightarrow {}^{60}_{28}\mathrm{Ni}^* + \gamma(1173.2\,\mathrm{keV}) \qquad I_{\gamma 1} \approx 99.9\%,$$

$$^{60}_{28}\mathrm{Ni}^*(1332.5) \rightarrow {}^{60}_{28}\mathrm{Ni} + \gamma(1332.5\,\mathrm{keV}) \qquad I_{\gamma 2} \approx 100\%.$$

Cesium-137:

$$^{137}_{55}\mathrm{Cs} \xrightarrow[T_{1/2}=30{,}018\ \text{years}]{\beta^-} {}^{137m}_{56}\mathrm{Ba} \xrightarrow[T_{1/2}=2{,}55\ \text{min}]{} {}^{137}_{56}\mathrm{Ba} + \gamma(661{,}7\ \mathrm{keV}) \qquad I_{\gamma 2} \approx 85.1\%.$$

Thorium-228:

$$^{228}_{90}\mathrm{Th} \xrightarrow[T_{1/2}=1{,}9116\ \text{years}]{\alpha} {}^{224}_{88}\mathrm{Ra} \ldots {}^{208}_{81}\mathrm{Tl} \xrightarrow{\beta^-} {}^{208}_{82}\mathrm{Pb} + \gamma(2614{,}5\ \text{keV}) \qquad I_{\gamma 2} \approx 99.75\% .$$

1.3 Neutron Interactions with Matter

The following processes are possible in interactions of neutrons with atomic nuclei:

1. Elastic scattering – the nucleus remains in its ground state; the neutron's energy is conserved in the center-of-mass frame;

2. Inelastic scattering – the nucleus is excited; the neutron's energy decreases;

3. Radiative capture – the neutron is absorbed by the nucleus, and the excitation is released via emission of γ rays;

4. Nuclear reactions in which nucleons or their fragments are emitted from the nucleus.

The radiative neutron-capture reaction (n, γ) proceeds as follows:

$$n + (A, Z) \rightarrow (A+1, Z)^* \rightarrow (A+1, Z) + \gamma .$$

Being an exoenergetic reaction, it proceeds on all nuclei (with the exception of $^{3}\mathrm{H}$ и $^{4}\mathrm{He}$ for which it is endoenergetic), starting from nucleus $^{1}\mathrm{H}$ and up to nucleus $^{238}\mathrm{U}$).

Elastic scattering (n, n) of neutrons does not change the internal state of the nucleus. In the center-of-mass frame (CM), the neutron's kinetic energy is conserved, whereas in the laboratory frame (LF) the total kinetic energy of the neutron–nucleus system is conserved. Two mechanisms of elastic scattering are distinguished—resonance scattering and potential scattering. Elastic scattering is the principal process of neutron moderation as neutrons propagate in matter.

Inelastic scattering (n, n') occurs when part of the neutron's kinetic energy is expended to excite the residual nucleus; consequently, the neutron emerging from the compound nucleus in the center-of-mass frame has less kinetic energy than the scattered neutron would have if the nucleus remained in its ground state. The inelastic scattering process can be schematically represented as follows:

$$n + (A, Z) \rightarrow (A+1, Z)^* \rightarrow (A, Z)^* + n' \rightarrow (A, Z) + n' + \gamma.$$

In neutron–nucleus interactions, resonances are observed that appear as narrow maxima in the cross section at specific energies.

For neutrons it is characteristic that resonances—narrow cross-section maxima—occur at certain energies. In the resonance-energy region, the reaction cross section is described by the Breit–Wigner formula [6]:

$$\sigma(E) = \frac{\pi}{k^2} \frac{g \cdot \Gamma_n \cdot \Gamma_{nr}}{(E - E_0)^2 + \frac{\Gamma^2}{4}},$$

where $k = 0.002197\sqrt{\frac{A}{A+1}E}$ – the neutron wave number in units of 10^{12} cm^{-1}; A – the mass number of the target nucleus; E_0 – the resonance energy; Γ_n – the neutron width; Γ_{nr} – the radiative width corresponding to the (*n, r*) reaction; $\Gamma = \Gamma_n + \sum_r \Gamma_{nr}$ – the total resonance width; $g = \frac{2J+1}{2(2I+1)}$ – the statistical weight, which depends on the target-nucleus spin (*I*) and the total angular momentum of the resonance *J*. The total angular momentum of the resonance is the vector sum of the target-nucleus spin *I*, the orbital angular momentum *l* and the neutron spin s_n:

$$\vec{J} = \vec{I} + \vec{l} + \vec{s}_n .$$

If the orbital angular momentum $l = 0$, the resonances are called *s*-resonances, $l = 1 - p$ −resonances, $l = 2 - d$ – resonances, and so on. At low energies,*s*-resonances dominate.

2 Experimental Section

2.1 Study of Time-of-Flight Spectra and Calibration of the «Gamma-7» Setup

2.1.1 Description of the IREN Facility

IREN (the Intense Resonance Neutron Source) was used only in one of the measurements – the energy calibration of the time-of-flight spectra, where it provided a pulsed neutron flux. The facility is currently undergoing maintenance and upgrades, so work with it is limited.

The LUE-200 electron linear accelerator, developed at the G. I. Budker Institute of Nuclear Physics, SB RAS (Novosibirsk), serves as the driver for the intense pulsed resonance neutron source IREN. It comprises a pulsed electron gun, an accelerating system, RF power sources based on 10-cm-band klystrons with modulators, diagnostic systems with a broadband magnetic spectrometer, and a vacuum system. The accelerator is installed vertically in the building of the former IBR-30 facility at the FLNP, JINR [1].

2.1.2 Description of the «Gamma-7» Setup

As noted earlier, at the first stage the IREN facility produces a pulsed neutron flux generated by irradiating a thick tungsten target with bremsstrahlung γ radiation via the (γ, n) reaction. At the second stage, the «Gamma-7» setup, located on a 10 m flight path of IREN channel No. 4, is used to register γ radiation arising from radiative neutron capture. It is equipped with an array of BGO-crystal scintillation detector modules, which enables studies of the angular distributions of γ quanta emitted in radiative neutron capture at resonances, as well as analysis of sample elemental composition by the neutron resonance analysis method.

The «Gamma-7» prototype consists of seven independent BGO scintillation detectors. The detector geometry forms a circle with an inner channel for the neutron beam to pass through. The detectors are powered from an external stabilized high-voltage supply connected via specialized BNC connectors.

The main configuration of the detector system includes:

1. An array of seven BDEG-1307-2 scintillation γ-ray detection modules based on bismuth germanate (BGO) crystals;
2. A CAEN DT8033N high-voltage stabilized power supply, 8-channel programmable HV power supply;
3. A CRS-32 digitizer (Digital Signal Recorder);
4. An AKTAKOM ADS-2224T digital oscilloscope;
5. A personal computer (Linux Mint).

Data acquisition is performed with a digital data-collection system, the CRS-32 digitizer. The CRS-32 is an analog-to-digital converter that records measured voltages with time tagging into an intermediate memory. The digitized pulses can be read by the control electronics either in real time during data accumulation or saved to the computer's hard drive. The recorded data are stored as decoded data (.dec) files, which are then analyzed with more specialized software to produce histograms [7].

At present, the Gamma-7 setup is in a preliminary (pilot) operation phase. Its parameters and characteristics have been refined to meet requirements that evolved as experience was gained and new ideas emerged during the planning and execution of experiments.

2.1.3 Methods for Processing and Visualization of Experimental Data

Various software tools were used for processing and analyzing the experimental data. For most of the work, the primary operating system was Linux Mint. The digitized data produced by the CRS-32 digital data-acquisition system were transferred to the Romana software suite, where they were recorded in RAW and ROOT formats for subsequent analysis. The CRS-32 digitizer converted the pulses, which were streamed online to Romana.

Romana – a program for the accumulation, analysis, and visualization of experimental data developed at the FLNP, JINR by Yuri N. Kopach, Cand. Sci. (Phys.–Math.) – is built on the ROOT framework. The acquired data can be saved in RAW and DEC formats, or as one- and two-dimensional spectra in ROOT format. For subsequent analysis of RAW-format data, visualization of the recorded waveforms is provided. During processing, the following signal parameters are determined: (1) discriminator trigger time, (2) pulse amplitude, (3) pulse area (integral) within a specified time gate, (4) baseline level, and (5) pulse width. For visualization of results, function fitting, and preparation of figures for reports, the OriginPro package was used, which is convenient for presenting experimental data as graphical illustrations.

2.1.4 Time-of-Flight Method

In neutron physics, the time-of-flight (TOF) method is often used to determine a particle's energy. A detector that records neutrons (or secondary particles produced by neutron interactions in the sample) is placed at a distance l from a pulsed neutron source. The neutron energy is determined according to [6]:

$$E_n = \frac{5226.7 \cdot l^2}{t_{\mathrm{f}}{}^2},$$

where l – the flight-path length (m); $t_f = t_1 - t_0$ – the time of flight (μs); t_0 – the instant when the neutron crosses the start of the flight path; t_1 – the instant when the neutron reaches the detector.

is defined by a start signal generated by a fast detector located near the neutron source. A pulsed operating mode of the neutron source is required to timestamp the neutron emission. At the IREN facility, these pulses have a duration of 250-300 ns, with a repetition rate of 25 or 50 Hz at an average current of 5 μA [1].

2.1.5 Measurement Results

Potassium bromide (KBr) was used as the sample. γ radiation was recorded with the Gamma-7 spectrometer. On the 4th channel of the IREN facility, the flight-path lengths were 11 m and 16 m.

During the measurements, IREN operated at 50 Hz. The spectrometer acquisition was started with a timing offset of approximately 2 μs relative to the neutron time-of-flight reference at the source.

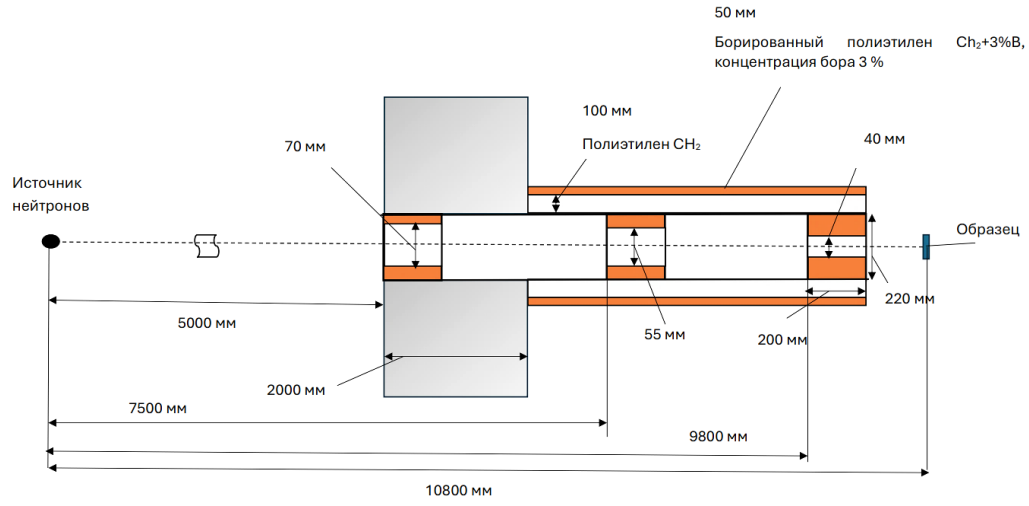

Figure 2 – Schematic of the 4th channel of the IREN facility.

The experiment measuring transmission through a KBr sample lasted 150 minutes. To monitor the radiation background, measurements were carried out in the working area. Data acquisition was performed using a CRS-32 digitizer, and data processing was done in the Romana program. After the measurements, the amplitude spectra were processed using the built-in software analysis tools.

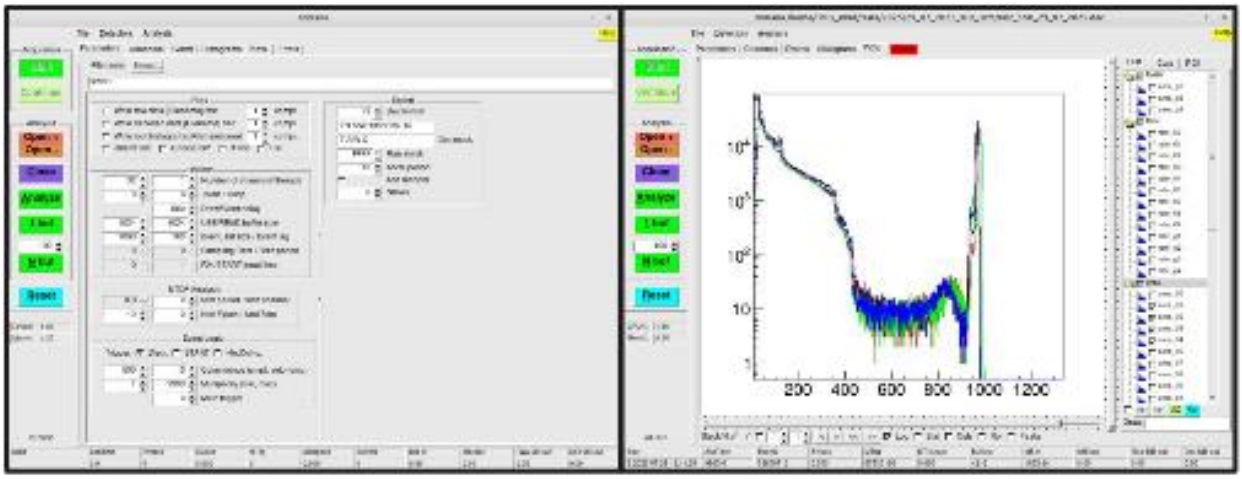

Figure 3 – Romana program interface and amplitude spectra obtained when measuring transmission through a KBr sample.

The neutron resonances observed in the spectra correspond to the isotopes Br-79 and Br-81.

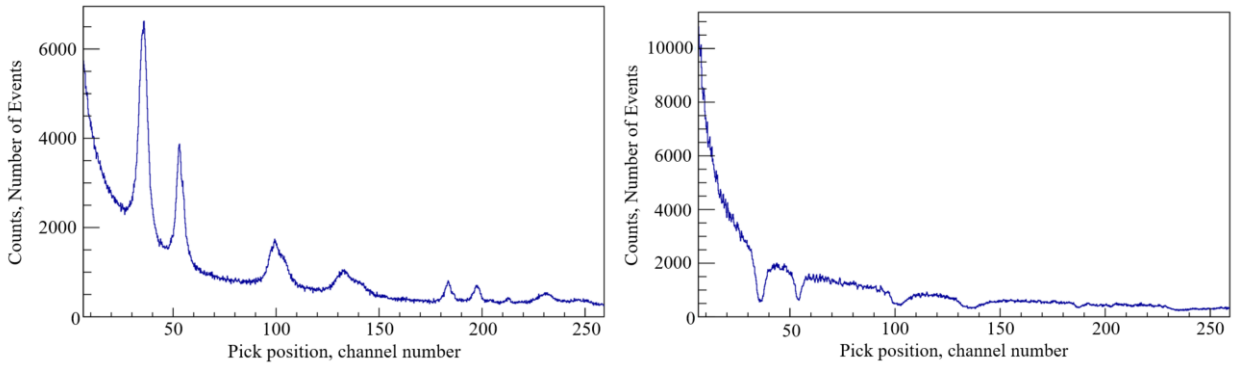

Figure 4 – Experimental spectra: left – radiative capture spectrum; right – transmission spectrum.

In the transmission spectrum, dips are observed that are associated with neutron capture by bromine nuclei in resonance energy intervals. In the radiative capture spectrum, pronounced peaks are recorded corresponding to radiative capture processes. These peaks reflect the emission of γ rays as nuclei transition from excited states to the ground state.

The results of the identified resonances are presented in Table 2. The methodology was based on comparing the experimentally obtained spectra with tabulated neutron resonance parameters [8], taking into account agreement in both energy and intensity.

Bromine isotope	E_0, **eV**	$2g\Gamma_n$, **meV**	Γ_γ, **meV**
Br-79	35.8(1)	53.9(54)	325
Br-79	53.6(9)	24.9(15)	390
Br-81	101.10(4)	195(14)	310
Br-81	135.60(5)	330(36)	–
Br-79	189.5(1)	55.0(55)	23.9

Table 2 – Identified resonances of Br-79 and Br-81.

2.1.6 Results of Determining the Start-Pulse Delay Time and the Flight-Path Length

To determine the start-pulse delay time t_0 and the flight-path lengths l_1, l_2, we used bromine resonances at 35.8 eV and 101.1 eV. From the positions of these peaks, four equations were obtained that relate l_1, l_2 and t_0:

$$\begin{cases} \dfrac{5226.7 \cdot l_1^2}{(133.6 - t_0)^2} = 35.8\ \text{keV} \\ \dfrac{5226.7 \cdot l_1^2}{(79.7 - t_0)^2} = 101.1\ \text{keV} \end{cases} \qquad \begin{cases} \dfrac{5226.7 \cdot l_2^2}{(197.5 - t_0)^2} = 35.8\ \text{keV} \\ \dfrac{5226.7 \cdot l_2^2}{(118.1 - t_0)^2} = 101.1\ \text{keV} \end{cases}.$$

The first two equations correspond to the flight path $l_1 = 11$ m, and the latter two to $l_2 = 16$ м. m. The delay time t_0 is the same for both paths.

The solution was carried out in Mathcad. Solving the system yielded the following values (Table 3):

Eliminated equation	l_1	l_2	t_0
$\frac{5226.7x^2}{(133.6-z)^2}=35.8$	10.922	16.248	1.171
$\frac{5226.7x^2}{(79.7-z)^2}=101.1$	10.96	16.248	1.171
$\frac{5226.7y^2}{(197.5-z)^2}=35.8$	11.016	16.343	0.492
$\frac{5226.7y^2}{(118.1-z)^2}=101.1$	11.016	16.305	0.492

Table 3 – Calculated values of the flight-path lengths l_1 and l_2 and the delay time t_0, obtained by solving the system of equations.

After the calculations and substitution of the obtained results into the Romana program, the exact values were obtained: the flight-path lengths were 10.96 m and 16.343 m. The delay time was 0.8315 μs.

2.1.7 Discussion of Results

Based on the determined flight-path lengths, it becomes possible to tackle problems such as identifying previously unknown resonances in new samples. One such task is determining a material's elemental composition. The key parameter in this case is the resonance energy, calculated from time-of-flight (TOF) data. The initial step that ensures a correct analysis is the precise determination of the time of flight and the flight-path length.

2.2 Determination of Detection Efficiency and Energy Resolution of the BGO Scintillation Detector

2.2.1 Characteristics of the BGO Detector

To measure the detection efficiency of the BGO detector, a 4π geometry was implemented. As the γ-radiation source (OSGI), Co-60 was chosen; it provides two spectral lines by which we determine the intrinsic efficiency. To achieve the 4π geometry, the OSGI source was placed between two detectors. Thus, for the efficiency determination we effectively realized only a quasi-4π geometry that does not cover the entire γ-emission solid angle.

The experimental measurements employed BDEG-1307-2 scintillation modules based on a bismuth germanate crystal $Bi_4Ge_3O_{12}$ (BGO), wrapped in a reflective sheath. The specifications of the BDEG-1307-2 detector are given in Table 4.

Detector	Length, cm	Height, cm	Operating temperature range, °C	Supple voltage, V
БДЭГ-1307-2	8.9	26.5	5-50	1000-1500

Table 4 – Specifications of the BDEG-1307-2 γ-radiation detection module.

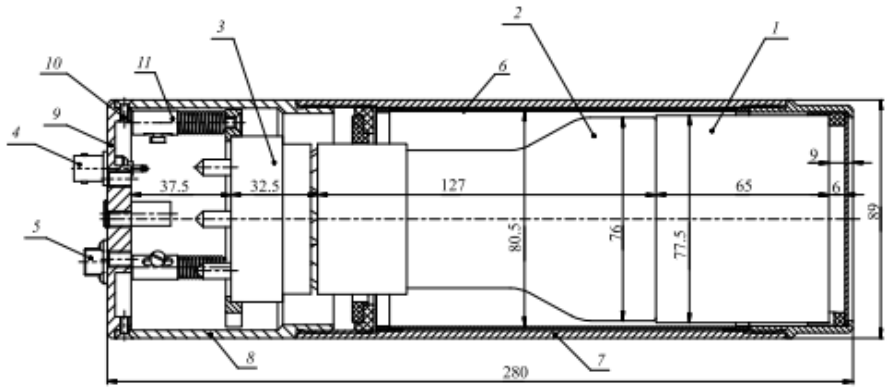

Figure 5 – Schematic of the BGO detector: 1 – BGO crystal; 2 – Hamamatsu R1307 PMT; 3 – voltage divider; 4 – power connector; 5 – signal connector; 6 – magnetic shield; 7 – detector housing; 8 – voltage-divider housing; 9 – rear cover with connectors; 10 – M3 screw; 11 – compression spring. All dimensions are in mm [8].

In the detector design, a Hamamatsu R1307 photomultiplier tube (PMT) is placed together with the crystal inside a detachable cylindrical aluminum housing 3 mm thick.

The Hamamatsu R1307 PMT is used to register scintillations and to form the electrical signal in the scintillation detector; its operating principle is based on photoelectric and secondary-emission conversion of light energy into an electrical signal. A necessary condition for the normal operation of a scintillation counter is the matching of the scintillator's emission spectrum to the spectral characteristic of the PMT photocathode.

2.2.2 Determination of the Activity of the Standard Gamma-Radiation Source (OSGI)

The "OSGI" sources were manufactured on September 1, 2019. By the time of the measurements on August 20, 2025, the source activity was lower than the initial value.

Calculation of the residual activity ^{60}Co at the time of the experiment:

$$A(t) = A_0 \cdot 2^{-t/T_{1/2}} = 96000 \cdot 2^{-1.662 \cdot 10^8 / 1.874 \cdot 10^8} = 43946.362\ Bq,$$

where $T_{1/2} = 5.2714$ years $= 1.874 \cdot 10^8\ s$ – the half-life ^{60}Co; $I_{\gamma 1}(1173.2\text{ keV}) = 0.9985$, $I_{\gamma 2}(1332.5\text{ keV}) = 0.9998$ – the γ-line intensities; $t = 5.9424\ years = 1.662 \cdot 10^8\ s$ – the elapsed time; $A_0 = 96000$ Bq – the initial activity per the datasheet.

At the time of measurement, the activity was $A = 43946.362$ Bq. This value is about half of the initial activity, yet still optimal for the registration conditions and for accumulating statistics.

2.2.3 Measurement Results

We established the required 4π geometry and performed measurements with a γ-ray source. To determine the detector efficiencies, we select the total events accumulated in the photopeaks at 1173 keV and 1332 keV. During the measurements, data were recorded using the Romana program. After the measurements, the obtained results need to be analyzed.

First, the background had to be measured. The average background recorded by the two detectors was $N_{bg,1} = 4685\ [counts]$; $N_{bg,2} = 4446$ [counts]. The number of background coincidences between the two detectors was also measured: $N_{bg,(2,3)} = 30$ [counts].

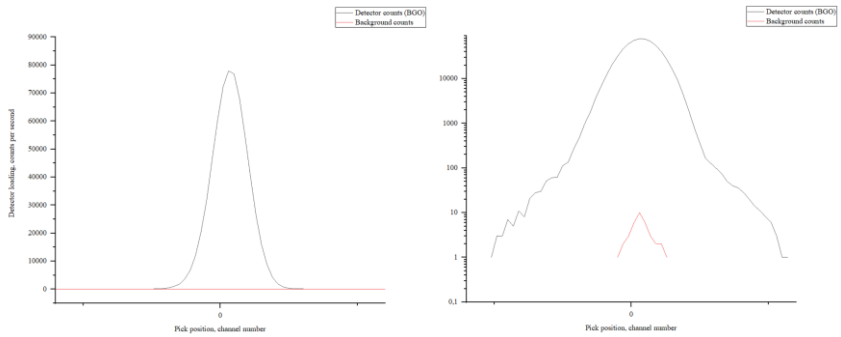

Figure 6 – Amplitude spectra of γ-radiation from the photopeaks ^{60}Co including the background contribution (red curve): left – linear scale; right – logarithmic.

2.2.4 Results of Determining the Intrinsic Efficiency of the BGO Detector

The numbers of γ quanta recorded by each detector, as well as the number of events in the coincidence spectrum, are presented. In forming the latter, one detector serves as the start detector, while signals from the second detector that occur within the coincidence time window upon the start trigger are recorded.

The numbers of γ quanta registered by each detector are N_1 and N_2, and the number in the coincidence spectrum is $N_{1,2}$. When forming the coincidence spectrum, one detector acts as the start, and events registered by the second detector upon its triggering are written to the spectrum. The formulas used for the calculation are:

$$N_1 = N_\gamma\,\varepsilon_1, N_2 = N_\gamma\,\varepsilon_2,$$

$$N_{1,2} = N_\gamma\,\varepsilon_1\,\varepsilon_2,$$

where N_1 и N_2 [counts] – the numbers of events in the peaks recorded by the respective detectors; $N_{1,2}$ [counts] – the number of coincidences between the detectors; N_γ [counts] – the total number of registered γ rays; ε_1, ε_2 [dimensionless] are the detection efficiencies for each detector.

The efficiency of each detector has its own value:

$$\varepsilon_1 = \frac{N_{1,2}}{N_2}, \qquad \varepsilon_2 = \frac{N_{1,2}}{N_1}.$$

Using the Romana program, the following results were obtained. Number of pulses recorded by the first detector: $N_{e1} = 2.968 \cdot 10^6$ [counts], number of pulses recorded by the second detector: $N_{e2} = 3.051 \cdot 10^6$ [counts] number of coincidences: $N_{e(2,3)} = 6.986 \cdot 10^5$ [counts] After background subtraction: $N_{i1} = 2.963 \cdot 10^6$ [counts]; $N_{i2} = 3.047 \cdot 10^6$ [counts]; $N_{i(2,3)} = 6.986 \cdot 10^5$ [counts].

Substitution gives:

$$\varepsilon_2 \approx \frac{6.986 \cdot 10^5}{3.047 \cdot 10^6} = 22.9\%, \qquad \varepsilon_3 \approx \frac{6.986 \cdot 10^5}{2.963 \cdot 10^6} = 23.6\%.$$

2.2.5 Discussion of Results

The intrinsic efficiency of both detectors was about $22 - 23\%$, which is consistent with the expected values for BGO scintillation crystals. This efficiency value reflects the detector's technical characteristics and is important for calibration.

It is important to note that even in an ideal 4π geometry – if a point-like source were located inside the detector's active volume – there are factors that preclude 100% detection. These may arise from the physical, design, and technological features of the instrumentation, the conditions of its use, as well as the individual qualities of the operator.

2.3 Identification of Lines in the Spectrum from a Neutron Source

2.3.1 Problem Statement and Experimental Procedure

Determining the positions of lines in spectra recorded by a spectrometer is an important task and depends directly on the accuracy of their energy calibration.

To first order, the relationship between the energy of the detected γ rays and the positions of the corresponding peaks is linear and can be written as

$$E_\gamma = a_0 + a_1 x,$$

where E_γ – energy in keV; x – the digitizer channel number; a_1 – the slope (keV/channel); a_0 – the intercept (keV).

To determine this dependence, it is sufficient for the spectrum to contain two reference peaks whose energies are known with adequate accuracy. Introducing a large number of reference lines into the spectrum is undesirable, as it either requires adding impurities to the measured spectrum or additionally acquiring a calibration spectrum; both reduce the accuracy of the energy determination.

In the γ-ray spectra we studied, clear peaks were observed from reactions ^{9}Be(α, n)^{12}C and from the γ-radiation of the sources $^{60}_{27}$Co, $^{137}_{55}$Cs, $^{228}_{90}$Th.

2.3.2 Processing of the Obtained Spectra: Energy Calibration of Amplitude Spectra

For calibration, the following reference lines were used: 661.7 keV, 1173.2 keV, 1332.5 keV, 2614.5 keV, 4.438 keV.

To improve accuracy, the entire measurement interval could be divided into several segments over which the linearity $E_\gamma(x)$ is adequately preserved. However, we used a global linear approximation together with a piecewise-linear one.

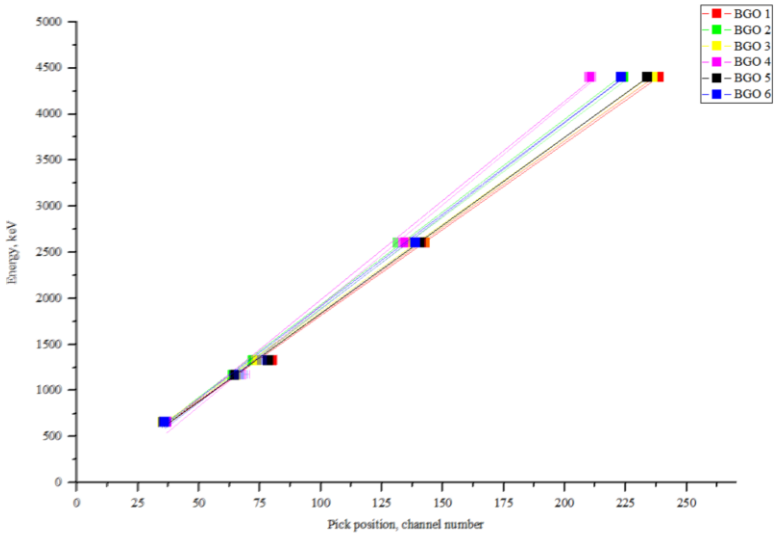

$$E_1(x) = -55.60 + 18.68 \cdot x_1$$
$$E_2(x) = -72.26 + 20.11 \cdot x_2$$
$$E_3(x) = -24.97 + 18.88 \cdot x_3$$
$$E_4(x) = -168.32 + 21.53 \cdot x_4$$
$$E_5(x) = -71.44 + 19.10 \cdot x_5$$
$$E_6(x) = -83.18 + 19.98 \cdot x_6$$

Figure 7 – Energy calibration of amplitude spectra for six BGO detectors; the calibration equations are shown on the right.

2.3.3 Processing and Discussion: Line Identification and Measurement Methodology

The width of the full-energy peak generally spans several channels for high-quality detectors; therefore, its position is determined by the centroid calculated about the axis of symmetry. Such peaks are satisfactorily approximated by the Gaussian function given earlier in Section 1.2.2.

It should be noted that the shape of a real peak does not exactly follow a Gaussian curve, and in lower-quality detectors deviations may appear as excess counts on the low-energy side of the peak (a tail). At high load or with insufficient instrument tuning, high-energy tails are sometimes observed. The upper portion of the peak corresponding to $50 - 70\%$ of its height is well described by a Gaussian distribution, which allows the peak position to be determined with sufficient accuracy [10].

There are various methods for determining peak positions in spectra. The simplest is the visual method: the peak position can be estimated by eye. However, this approach is approximate in nature and is used mainly for quick assessments. In this work, we employed spectral plotting and Gaussian fitting in OriginPro. A Gaussian function was used because the full-energy peaks considered here are theoretically described by a Gaussian distribution. Figure 8 shows the procedure used in this study to determine the position of the full-energy peak maximum.

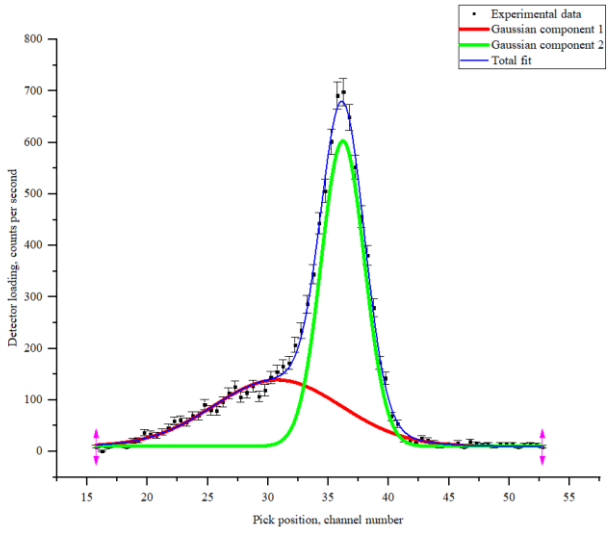

Figure 8 – Determination of the full-energy peak position in the Cs-137 spectrum measured with a BGO scintillator.

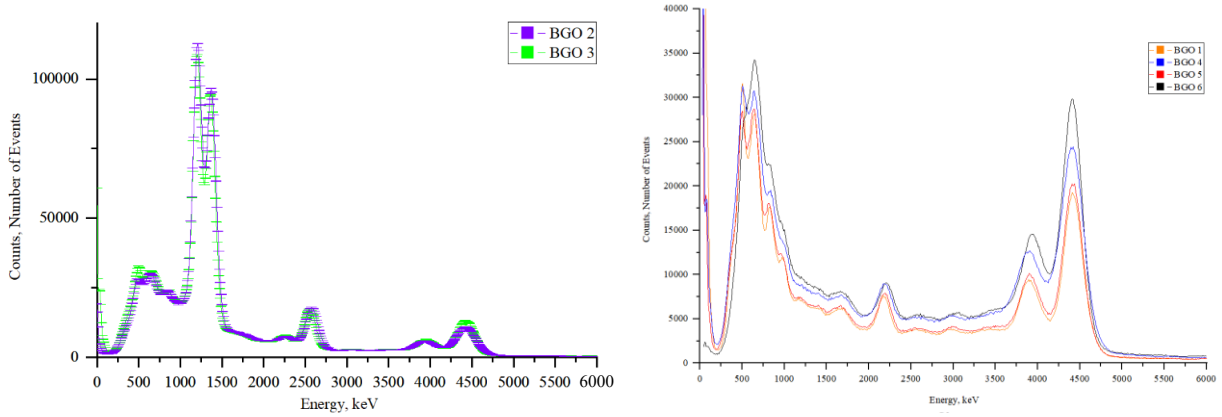

Figure 9 – Pulse-amplitude spectrum of the sources $^{60}_{27}\mathrm{Co}$, $^{137}_{55}\mathrm{Cs}$, $^{228}_{90}\mathrm{Th}$ and of the neutron source AmBe, measured with a BGO scintillator. Left – high load. Right – low load.

Figure 9 shows the calibrated amplitude spectra from the OSGI source and from the neutron source. Two BGO detectors operated at high load under “OSGI”. After calibration, the spectra from all detectors were aligned on the energy scale. In the high-load “OSGI” spectra, one can see the channels where the full-energy peaks of Co-60 are located. The thorium peak at 2264 keV is also visible, which is rather difficult to observe in the spectra recorded with the other detectors.

Identification of γ-ray lines in the experimental spectra was performed using the NNDC (National Nuclear Data Center) database [9], which is one of the principal global sources for the collection, processing, and dissemination of nuclear data. The analysis revealed antimony lines originating from the lead bricks used as radiation shielding. In addition, it was established that the temperature regime in the fourth channel of the IREN facility has a noticeable effect on the measurement results. Figure 10 presents the identified peaks corresponding to Cs-137, Co-60, Th-228, as well as lines arising from neutron interactions with beryllium. The spectra clearly exhibit Compton continua, the e^+e^- annihilation peak, and the single- and double-escape peaks.

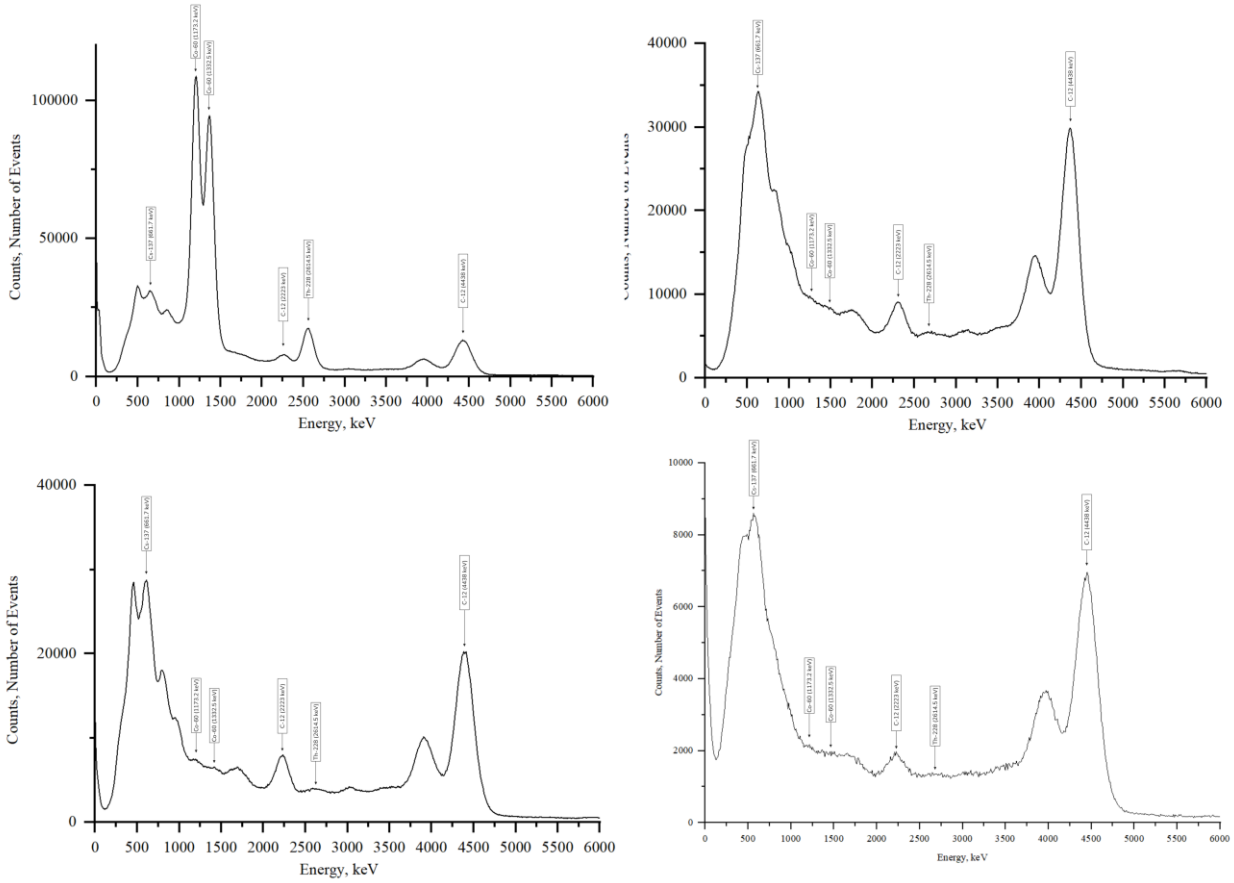

Figure 10 – Amplitude spectra obtained with the gamma-ray sources $^{60}_{27}\mathrm{Co}$, $^{137}_{55}\mathrm{Cs}$, $^{228}_{90}\mathrm{Th}$ and with the AmBe neutron source at different detector load levels.

2.4 Study of the Temperature Dependence of Resolution and Recorded-Signal Amplitude of the BGO Scintillation Detector

2.4.1 Problem Statement and Measurements

The most important characteristics of a scintillator for gamma-ray spectrometry are mechanical robustness, high light yield, sufficiently high density, and temperature stability of the light output.

During long measurements it was noted that temperature variations on the 4th channel of the IREN facility have a significant effect on the stability of the recorded spectra. Daytime temperature changes led to peak shifts, changes in peak width, and degradation of the energy resolution. Accordingly, one of the objectives was to investigate the temperature dependence of the spectrometric parameters in order to determine the optimal operating conditions for the detectors.

2.4.2 Results on Temperature Dependence

To address this task, an experimental setup was assembled consisting of two BGO scintillation detectors mounted in a quasi-4π geometry, a liquid-nitrogen cooling system, lead blocks to provide thermal mass, and a digital thermometer with a thermocouple and an ADC. A heating element was additionally used to probe the upper temperature range.

Before feeding the detector signals to the CRS-32 (digital signal recorder) digitizer, the permissible input amplitude and pulse shape must be verified: peak-to-peak (Vpp), rise/fall time, and noise/pickup. The CRS-32 has an operating input range of approximately ±1 V with a 50 Ω input. Exceeding this range leads to ADC saturation and waveform distortion, and may damage the input stage [7].

Cs-137 was used as the source of γ-radiation. The acquisition time at a relatively fixed temperature (±1 °C) was $t_i = 30$ s. The recorded spectra were processed by fitting a Gaussian function in OriginPro. We determined the signal amplitude and the detector resolution σ for the thorium and cesium lines in channel units. During the measurements, one detector operated at a load of 16000 counts/s, and the other at 11000 counts/s.

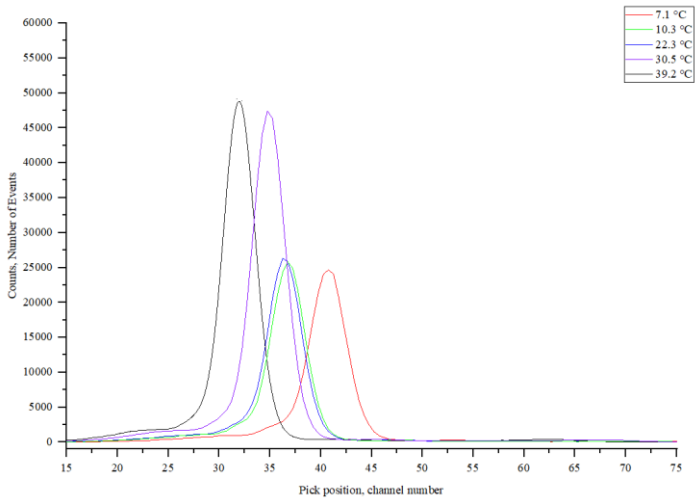

Figure 11 – Amplitude spectra of the photopeak ^{137}Cs at 661.7 keV on the digitizer's channel scale, acquired at different temperatures (see legend).

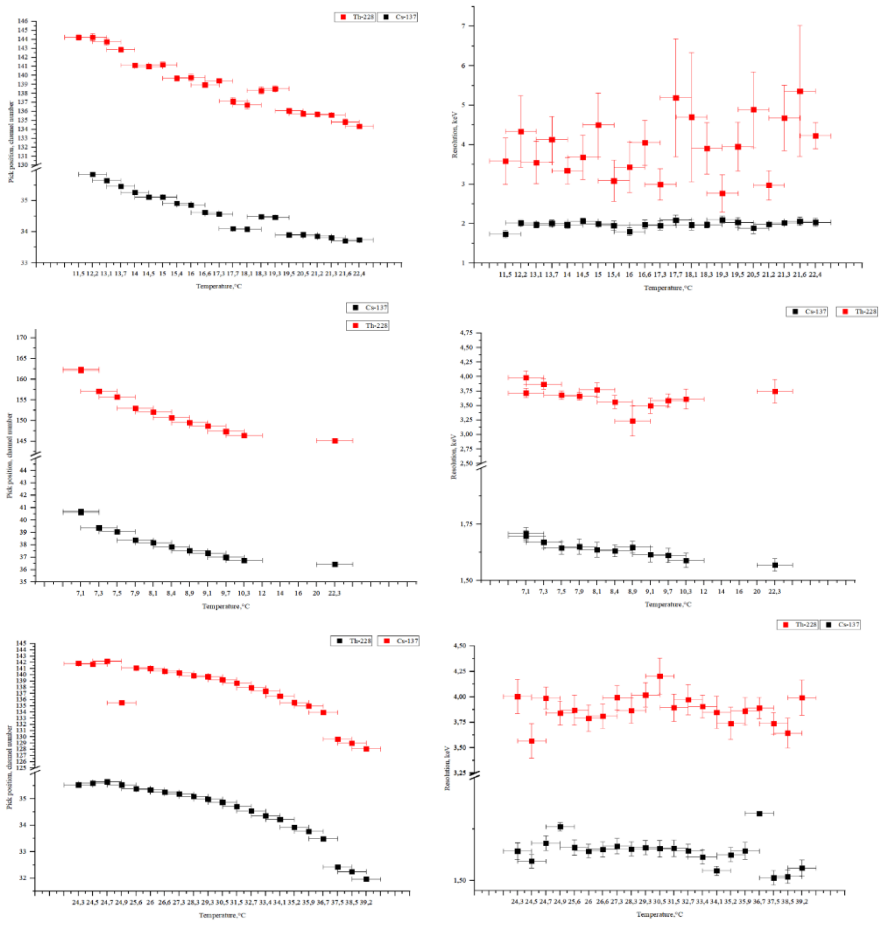

Figure 12 – Temperature dependences of the peak position (channel scale; left) and energy resolution (right) for the photopeaks at ^{137}Cs 661.7 keV ^{228}Th and 2614.5 keV at detector loads of 300, 10000, and 16000.

2.4.3 Discussion of Results

Figures 11 and 12 show that, for spectra taken at different temperatures, the full-energy peak ^{137}Cs (661.7 keV) is shifted along the channel scale by $2.5 - 7$ channels (the channel width in these measurements was 18.8 ± 0.4 keV) between the nearest and the most displaced centroid positions. There is also a noticeable change in the shape of the peak – its width and height. This change arises from differences in detector load during the heating and cooling runs, which is determined by the experimental conditions of the setup. For a precise analysis, it is necessary to perform measurements at identical load for all temperatures or to normalize for acquisition time and peak area. The energy drift of the centroid with changing temperature may result from a decrease in PMT sensitivity rather than the BGO light yield, since the temperature dependence of the scintillation intensity contributes mainly at higher temperatures (from about 50 °C), which we did not reach [11].

2.5 Study of the Influence of Count Rate (Load) on the Characteristics of the «Gamma-7» Setup

2.5.1 Problem Statement and Measurements

The changes in energy resolution and peak positions observed in previous experiments suggested a dependence of the recorded spectra on the counting load. The objective of this measurement was to quantify the effect of load on energy-scale drift and on the degradation of the energy resolution of the «Gamma-7» setup. To investigate the variation of resolution as a function of detector load, we used a “OSGI” and an AmBe source, placing them at different distances from the detector.

The following reference lines were used: ^{60}Co – 1173 and 1332 keV, the coincidence peak – 2505 keV, and the γ-ray line – 4438 keV. The energy dependence of the resolution was approximated by the following expression:

$$\sigma(E) = \sqrt{a_0 + a_1 E + a_2 E^2},$$

where a_0, a_1, a_2 — fit parameters, E – γ-ray energy. For the BGO detector, the fitted parameters were: $a_0 = 2.2769$ кэВ^2 , $a_1 = 5.527 \cdot 10^{-4}$ кэВ, $a_2 = 1.051 \cdot 10^{-7}$.

2.5.2 Results for Resolution and Recorded-Signal Amplitude versus Detector Count Rate (Load)

Figure 13 shows that, as the detector load was varied, the energy resolution degraded by $1.5 - 3$ channels (the channel width in these measurements was 20.807 ± 0.1 keV). At the same time, the peak positions remained unchanged. A systematic deterioration of the energy resolution was observed with increasing detector load. At a load of about 27000 counts/s, an uncharacteristic rise (worsening) is observed. This effect is most likely due to limitations of the digitization chain combined with possible PMT nonlinearities. A further increase in count rate proved impossible under the experimental conditions: the maximum achieved load was roughly 42000 counts/s.

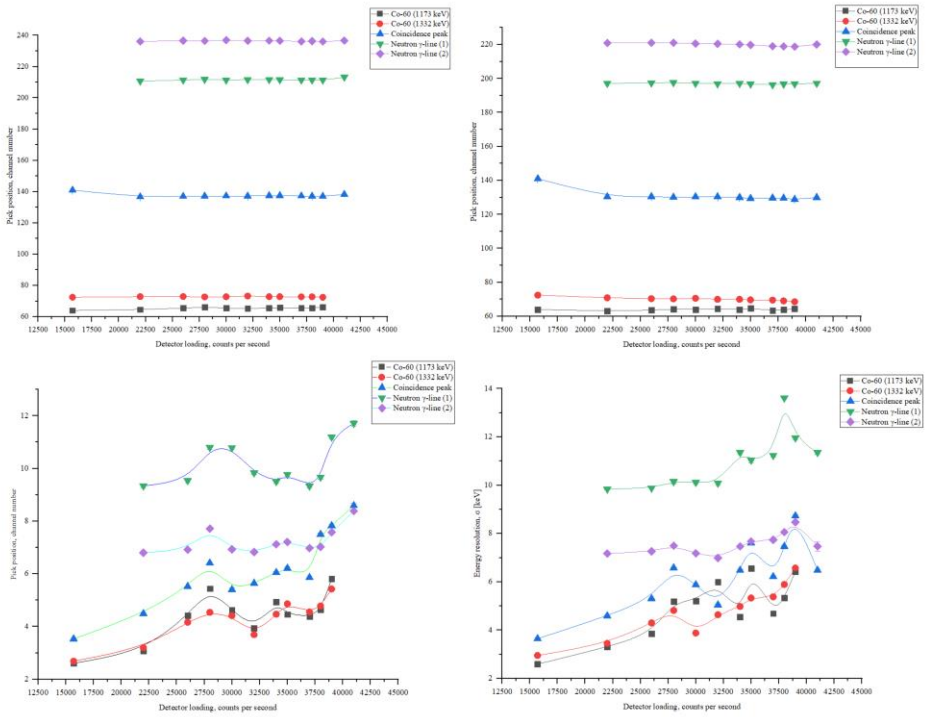

Figure 13 – Dependence of the peak positions of the γ lines (1173 and 1332 keV), the coincidence peak, and the neutron lines on the detector count rate (load) (top row), and the corresponding values of the standard deviation/energy resolution (bottom row).

In this experiment, we also set out to verify on our own BGO detectors an interesting result obtained by the TANGRA project research group [13].

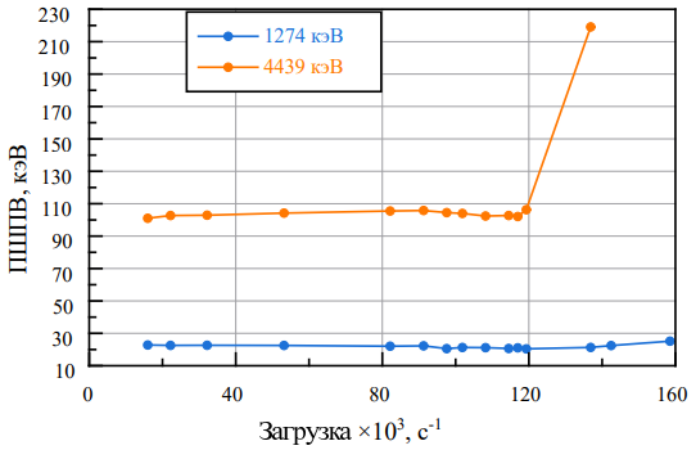

Figure 14 – Dependence of the energy resolution at the 1274 keV and 4439 keV peaks on detector load (based on data from the TANGRA project).

In their work, for the γ lines at 1274 and 4439 keV, the dependence of the full width at half maximum (FWHM) on detector load was plotted (Fig. 14). For the high-energy 4439 keV line, a sharp degradation of the resolution is observed at count rates above 120000 counts/s, whereas for 1274 keV the dependence is weaker. This effect is of considerable interest, and we attempted to reproduce it on the «Gamma-7» setup.

Conclusions

Over the course of the internship, we conducted five experiments on the prototype of the «Gamma-7» setup. The results obtained made it possible to confirm in practice the theoretical concepts of γ-ray spectroscopy using scintillation detectors, including the need for their calibration and the consideration of external conditions that affect detector sensitivity.

Determining the time of flight and the flight-path length introduced the time-of-flight method and provided a basic calibration of the setup. Measurements with the Co-60 “OSGI” in a quasi-4π geometry yielded an intrinsic detection efficiency of the BGO scintillation detectors of 22-23%, which is consistent with the expected characteristics of bismuth germanate crystals. The identification of gamma-ray lines from standard calibration sources allowed us to determine characteristic nuclear transitions and gain experience in calibrating spectra and working with databases. Examining the temperature dependence allowed us to assess the influence of external conditions on the stability of the detector response.

In the course of the work, we improved our skills in processing experimental data using Mathcad, Romana, and Origin, as well as working in the Linux Mint operating system.

Overall, the measurements provided a coherent picture of the operation of scintillation detectors. Work with the prototype of the «Gamma-7» setup confirmed its potential for further research. The setup remains in the initial commissioning phase, and the results obtained can be used to improve and expand its operating parameters and performance characteristics.

References

1. Joint Institute for Nuclear Research (JINR). IREN Resonance Neutron Source [Electronic resource]. — URL: https://flnp.jinr.int/ru/glavnaya/ustanovki/iren (accessed September 14, 2025).

2. Joint Institute for Nuclear Research (JINR). Patent for the “Romana” software for accumulation, analysis, and visualization of experimental data [Electronic resource]. — URL: https://www.jinr.ru/posts/patent-na-programmu-nakopleniya-analiza-i-vizualizatsii-eksperimentalnyh-dannyh-romana/ (accessed August 16, 2025).

3. OriginLab Corporation. Origin — Data Analysis and Graphing Software [Electronic resource]. — URL: https://www.originlab.com/ (accessed August 5, 2025).

4. State Scientific Center of the Russian Federation — A. I. Leypunsky Institute for Physics and Power Engineering (IPPE). Am-241–Be neutron sources [Electronic resource]. — URL: https://www.ippe.ru/production/isotopes/1218-neutron-sources-am241-be (accessed August 20, 2025).

5. Institute of Nuclear Physics, Siberian Branch of the Russian Academy of Sciences (INP SB RAS). Description of laboratory exercises for the “Nuclear Practicum” / INP SB RAS. — Novosibirsk, 2010. — 112 pp.

6. Borzakov, S. B. Measurements of Neutron Resonance Parameters: internal report / S. B. Borzakov. — Dubna: Joint Institute for Nuclear Research (JINR), 2022. — 13 pp.

7. Joint Institute for Nuclear Research (JINR). Scientific Achievements of JINR [Electronic resource]. — URL: https://www.jinr.ru/posts/99076/ (accessed August 18, 2025).

8. Fedorov, N. A. Inelastic Scattering of Fast Neutrons by the Nuclei of Magnesium, Aluminum, Silicon, and Iron: Candidate of Sciences (Physics and Mathematics) dissertation / N. A. Fedorov; Lomonosov Moscow State University. — Moscow, 2021. — 156 pp.

9. National Nuclear Data Center. Brookhaven National Laboratory [Electronic resource]. — URL: https://www.nndc.bnl.gov/ (accessed August 18, 2025).

10. Shendrik, R. Yu. Introduction to the Physics of Scintillators—2: study guide / R. Yu. Shendrik, E. A. Radzhabov. — Irkutsk: Irkutsk State University Press, 2014. — 95 pp. — (Methods of Experimental Physics of Condensed Matter). — ISBN 978-5-9624-1104-0.

11. Belousov, A. A.; Zlygostev, I. N. Methodology for correcting for scintillator temperature instability in a portable gamma spectrometer for exploration geophysics. A. A. Trofimuk Institute of Petroleum Geology and Geophysics, Siberian Branch of the Russian Academy of Sciences; Novosibirsk State Technical University. Novosibirsk, 2020. 12 pp.

12. Shendrik, R. Yu. Mechanisms of excitation-energy transfer in alkaline-earth fluoride crystals doped with cerium and praseodymium ions: Candidate of Physical and Mathematical Sciences dissertation (specialty 01.04.07). A. P. Vinogradov Institute of Geochemistry, Siberian Branch of the Russian Academy of Sciences. Irkutsk, 2011. 148 pp.

13. Kharlamov, P. I.; Grozdanov, D. N.; Prusachenko, P. S.; Fedorov, N. A.; Kopach, Yu. N.; Tretyakova, T. Yu.; Pampushik, G. V.; Andreev, A. V.; Skoy, V. R.; Khramko, K.; Ruskov, I. N. Gamma-detector characteristics in the TANGRA project facility. Joint Institute for Nuclear Research; Lomonosov Moscow State University; Institute for Nuclear Research and Nuclear Energy, Bulgarian Academy of Sciences. Dubna—Moscow—Sofia, 2019. 16 pp.